Mater Struct (2024) 57:63
https://doi.org/10.1617/s11527-024-02302-4

ORIGINAL ARTICLE

# Effects of the geometric characteristics of graphene nanoplatelets on the physico-rheological properties of asphalt binder

**Hashem Khaled Almashaqbeh · Grace Rushing · Jesse Doyle · Dineshkumar Sengottuvelu · Mohammed Majdoub · Ahmed Al-Ostaz · Hunain Alkhateb · Sasan Nouranian · Mine G. Ucak-Astarlioglu**

Received: 25 August 2023 / Accepted: 12 January 2024


**Abstract** While graphene nanoplatelets (GnPs) have emerged as promising nano-modifiers of asphalt binder in recent years, much is still unknown in terms of the existing correlations between the physical, chemical, and geometric characteristics of this nanofiller and observed asphalt binder properties. In this work, we investigate the important correlation between the geometric characteristics of GnPs and the rheological properties of the GnP-modified asphalt binder at high temperatures. Our results indicate that, in general, incorporating GnPs with large mean particle diameters (> 14 μm) and thicknesses (> 8 nm) enhances the high-temperature performance of the asphalt binder. The results of the multiple stress creep and recovery tests confirm that including GnPs in asphalt binder can decrease its permanent deformation by 33.2% and enhance its elastic recovery by 53.9%. Phase contrast images obtained by atomic force microscopy further indicate that the presence of GnPs with large mean particle diameters alters the morphology of the asphalt binder, leading to improved temperature stability and less susceptibility to permanent deformation.

**Keywords** Graphene nanoplatelets · Asphalt binder · Particle diameter · Rheological properties · Multiple stress creep and recovery test · Atomic force microscopy

H. K. Almashaqbeh · G. Rushing · D. Sengottuvelu · M. Majdoub · A. Al-Ostaz (✉) · H. Alkhateb · S. Nouranian
Center for Graphene Research and Innovation, University of Mississippi, University, MS 38677, USA
e-mail: alostaz@olemiss.edu

H. K. Almashaqbeh · G. Rushing · A. Al-Ostaz · H. Alkhateb
Department of Civil Engineering, University of Mississippi, University, MS 38677, USA

J. Doyle · M. G. Ucak-Astarlioglu
Engineer Research and Development Center, U.S. Army Corps of Engineers, Vicksburg, MS 39180, USA

S. Nouranian
Department of Chemical Engineering, University of Mississippi, University, MS 38677, USA

Published online: 13 April 2024

## 1 Introduction

Enhancing the high-temperature properties of asphalt binders is imperative for prolonging the lifespan of asphalt roadways and minimizing the associated maintenance costs. One of the most common approaches to enhance the performance of asphalt binders at high temperatures is through the addition of modifiers such as rubbers [1–3], polymers [4–6] and, recently, nanomaterials [7–9]. Nanomaterials have shown great promise in improving various properties of asphalt binders, such as high-temperature performance, thanks to their large surface area and unique physicochemical properties [10]. Examples of nanomaterials used to modify asphalt binders include

nano-$TiO_2$ [9, 11, 12], nano-clays [13, 14], nano-silica [15], nano-ZnO [16], carbon nanofibers [17, 18], carbon nanotubes [19, 20], and more recently graphene [10, 21]. These nanomaterials offer promising prospects for enhancing asphalt binder performance, and the unique characteristics of graphene have received a lot of interest in recent research efforts [7, 10, 19, 22]. For example, Li et al. [10] examined the effect of graphene on the high-temperature performance of asphalt binders at different aging conditions. Their results indicated that adding 1 wt% graphene to asphalt binder can significantly enhance its aging resistance and improve its thermal stability. Nazki et al. [21] reported that graphene can increase the complex shear modulus and reduce the phase angle of asphalt binder. In research conducted by Brcic [23], it was observed that incorporating graphene at a concentration of 2 wt% dramatically reduces the permanent deformation of the asphalt binder. Similarly, Navarro et al. [24] reported that graphene obtained from the reduction of graphene oxide can enhance the elastic response and reduce the thermal susceptibility of asphalt binders when incorporated at an optimal content of 0.5 wt%. Despite the existing efforts to improve the performance of asphalt binders by the inclusion of graphene or its derivatives in its formulation, the evaluation of the physical, mechanical, and chemical characteristics of graphene-modified asphalt binders remains to be elucidated. In fact, determining the optimal content of graphene based on its geometric and chemical characteristics is needed to target the design of performance-grade engineered asphalt. Based on the available literature, the optimal graphene content ranges from 0.01 to 3 wt% [10, 21, 23–30]. This wide range becomes significant given the substantial cost associated with such nanomaterials. The uncertainty in the reported optimal graphene content might be related to the variability in the physical and chemical characteristics of graphene used for asphalt binder modification as well as the modification methods. Among these variables, the geometric characteristics of graphene on the behavior of the modified asphalt binder are hypothesized to be most influential. Utilizing graphene without considering its geometric characteristics may result in misleading findings or, at the very least, limit the potential outcome derived from employing graphene as an asphalt binder modifier.

Several research efforts have been undertaken to comprehend the underlying mechanisms behind graphene-enhanced asphalt performance, but conclusions remain ambiguous. The literature consensus is that when graphene is added to asphalt binder, the interlayer distance of asphaltene, a main component of asphalt binder, increases, thereby enabling the insertion of stiff and strong GnPs in its place and contributing to the overall enhancement of asphalt binder performance [28, 31, 32]. Another hypothesis suggests that graphene acts as a micellar center, impeding particle mobility and augmenting the viscosity of the asphalt binder [10, 22, 33]. Nevertheless, to date, there is no clear elucidation of how graphene or its derivatives truly improve the asphalt binder performance.

In light of the above discussion, it is important to establish a correlation between the graphene characteristics, such as mean particle diameter and surface area, and the high-temperature performance of graphene-modified asphalt binder. Addressing these tasks can unlock the potential for maximizing the performance of modified asphalt binders in extreme temperatures, both high and low, by incorporating graphene or its derivatives as modifiers for asphalt binders. In this study, we investigated the high-temperature performance of asphalt binders modified with four different GnP sizes and various GnP contents. For this purpose, a total of 14 binder specimens were tested under two different conditions (unaged and aged) following the AASHTO standards. The impact of the GnP mean particle diameter and surface area on the performance of an asphalt binder was evaluated by the rotational viscosity, rutting parameter, and multiple stress creep and recovery (MSCR) tests. Moreover, atomic force microscopy (AFM) and Fourier transform infrared (FTIR) spectroscopy measurements were performed to understand the physico-chemical role of GnPs in improving the high-temperature performance of the asphalt binder.

## 2 Materials and methods

### 2.1 Materials

Asphalt binder (PG 67-22, performance grade) was provided by Ergon, Inc, Jackson, MS, United States. Four GnP powder grades, i.e., xGnP® M15, M25,

R25, and C750, were purchased from XG Sciences, Inc, Lansing, MI, United States. The M15 and M25 grades have similar thicknesses and surface areas but differ in their lateral dimensions or "particle diameters," while the M25 and R25 grades have similar lateral dimensions but differ in their thicknesses and surface areas. The C750 grade has a very small mean particle diameter and an exceptionally high surface area. The geometric characteristics of the xGnP® grades used in this study are listed in Table 1.

## 2.2 Sample preparation

The GnP-modified asphalt binder samples were prepared using the direct addition method. First, the binders were conditioned in an oven at a temperature of 160 °C for 45 min. Next, the GnP powders in the content range of 0.05–2.0 wt% (Table 2) were added to the conditioned asphalt binders and rigorously mixed using a high-shear mixer (L5M-A Laboratory Mixer, Silverson Machines, United Kingdom) at a rotational speed of 9000 rpm for 45 min to ensure uniform dispersions of the GnPs in the binders. The temperature was maintained at 160 °C during the mixing process. The sample formulations and their assigned codes are listed in Table 2.

**Table 1** Geometric characteristics of the xGnP® grades used in this study

| Geometric characteristics | M15 | M25 | R25 | C750 |
|---|---|---|---|---|
| Surface area ($m^2/g$) | 128.30 | 132.80 | 41.30 | 750 |
| Mean particle diameter (μm) | 14.36 | 24.32 | 24.10 | 0.81 |
| $D_{10}$[a] (μm) | 3.89 | 5.74 | 5.54 | 0.35 |
| $D_{50}$[a] (μm) | 12.01 | 19.42 | 18.35 | 2.25 |
| $D_{90}$[a] (μm) | 28.07 | 50.58 | 51.55 | 4.76 |
| $D_{max}$[b] (μm) | 110.20 | 220.70 | 254.58 | 29.73 |
| Thickness (nm) | 6–8 nm | 6–8 nm | > 15 nm | < 2 nm |

[a]$D_{10}$, $D_{50}$, and $D_{90}$ are defined as the points on the particle size distribution curve below which 10, 50, and 90% of the nanoparticles fall, respectively

[b]Maximum particle size

**Table 2** Sample formulations and their assigned codes. All samples contain the PG 67-22 asphalt binder

| Sample no | Sample Code | GnP Powder Grade | GnP Content (wt%) |
|---|---|---|---|
| 1 | Control | - | 0 |
| 2 | 0.05 M15 | M15 | 0.05 |
| 3 | 0.1 M15 | M15 | 0.1 |
| 4 | 0.5 M15 | M15 | 0.5 |
| 5 | 1.0 M15 | M15 | 1.0 |
| 6 | 1.5 M15 | M15 | 1.5 |
| 7 | 2.0 M15 | M15 | 2.0 |
| 8 | 0.025 C750 | C750 | 0.025 |
| 9 | 0.05 C750 | C750 | 0.05 |
| 10 | 0.1 C750 | C750 | 0.1 |
| 11 | 0.5 C750 | C750 | 0.5 |
| 12 | 1.0 C750 | C750 | 1.0 |
| 13 | 1.0 M25 | M25 | 1.0 |
| 14 | 1.0 R25 | R25 | 1.0 |

## 2.3 Characterization

The performance of the samples (Table 2) was evaluated at two different conditions, i.e., unaged and short-term aged, which are outlined in Fig. 1. The details of each characterization method are provided next.

### *2.3.1 Rotational viscosity*

The rotational viscosities of the unaged neat and GnP-modified binder samples were measured at 120, 135, 150, and 165 °C using an FGB EVO-Series rotational viscometer (New South Wales, Australia), as per the AASHTO T-316 standard.

### *2.3.2 Rheometry*

The rheological properties (dynamic shear) of the neat and GnP-modified binder samples were evaluated at 64, 70, and 76 °C using a Rheotest DSR RN 4.3 rheometer (Germany), following the AASHTO T-315 standard. The dynamic shear rheometer (DSR) test provides the complex shear modulus (G*) and phase angle (δ) of the unaged and short-term aged binders. A parallel plate with a diameter of 25 mm was utilized to measure the rutting parameter, i.e., G*/sin(δ). Specifically, the test was performed at a

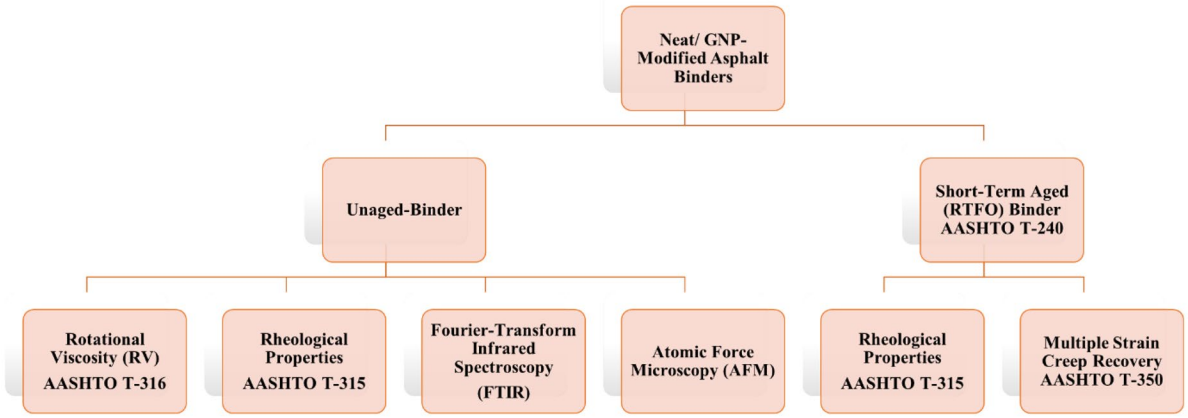


**Fig. 1** Characterization scheme for the samples

temperature of 64 °C. Then, the temperature gradually increased by 6 °C intervals until the rutting parameter value was lower than 1.00 and 2.20 kPa for the unaged and short-term aged binders, respectively.

### *2.3.3 Multiple stress creep and recovery*

The multiple stress creep and recovery (MSCR) test was performed to determine the rutting resistance by measuring the creep and recovery behavior of the neat and GnP-modified binders. The test was conducted on the short-term aged binders at 64 and 70 °C following the AASHTO T-350 standard. Cyclic constant creep stress with two different stress levels, including 0.1 and 3.2 kPa, were applied to the samples for 1 s, followed by a recovery period of 9 s. Then, the results obtained from the DSR test were used to calculate the non-recoverable creep compliance ($J_{nr}$) and percent recovery ($R_{\%}$) at each stress level.

### *2.3.4 Fourier-transform infrared spectroscopy*

The chemical structures of aged and unaged GnP-modified binders were investigated with Fourier-transform infrared spectroscopy (FTIR) using a Cary 630 FTIR instrument (Agilent Technologies, Santa Clara, CA, United States) with a Golden Gate single reflection attenuated total reaction (ATR) accessory. The FTIR Spectra were recorded in the range of 650–4000 $cm^{-1}$ at a resolution of 32 $cm^{-1}$. All spectra were obtained after an accumulation of 32 scans.

### *2.3.5 Atomic force microscopy*

The sample morphologies were investigated with a Dimension XR Scanning Probe Microscope and Icon scan head (Bruker Nano Inc., Santa Barbara, CA, United States) in tapping mode with a TESPA-V2 probe. The height and phase contrast images (40×40 μm) were analyzed with Gwyddion (version 2.62), an open-source data analysis and visualization software for scanning probe microscopy. The AFM samples were prepared by placing a bead of the binder on a glass microscope slide, which was heated in an oven at 160 °C for 20 min and then cooled to room temperature prior to imaging.

## 3 Results and discussion

### 3.1 Rotational viscosity

The effect of the GnP geometric characteristics/content on the viscosity of the unaged asphalt binder samples at different temperatures is illustrated in Fig. 2. For the M15 GnPs, the viscosity of the binders increases as the GnP content increases at all tested temperatures (Fig. 2a). For example, at the testing temperatures of 120, 135, 150, and 165 °C, adding 2.0 wt% M15 GnP to the asphalt binder results in rotational viscosity increases of 90.9, 71.3, 81.1, and 74.7%, respectively. In contrast, the influence of the C750 GnP with the smallest mean particle diameter and largest surface area on the rotational viscosity of

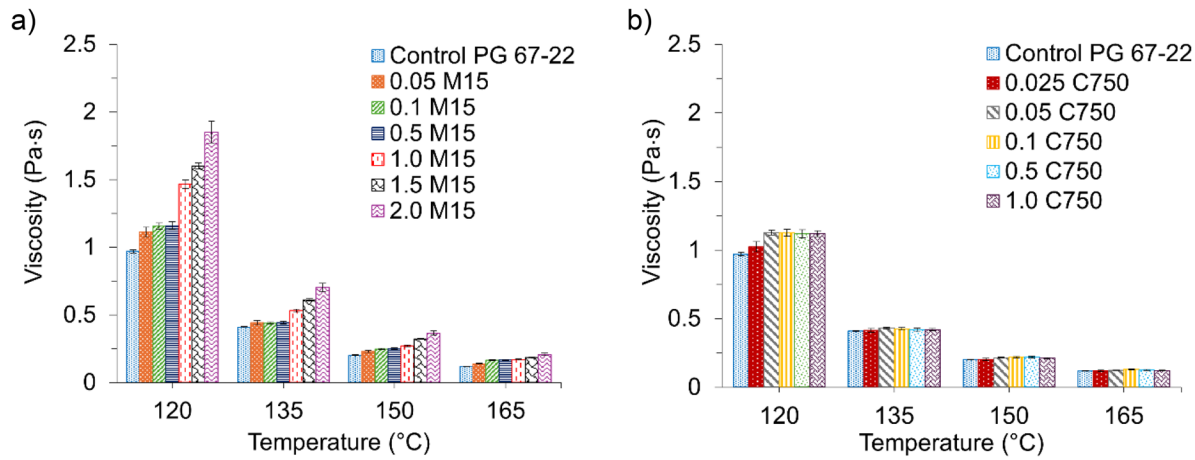


**Fig. 2** Effects of the different contents of **a** M15 GnPs and **b** C750 GnPs on the rotational viscosity of the PG 67-22 asphalt binder at different temperatures

the asphalt binder is found to be limited (Fig. 2b). At a temperature of 120 °C, a slight increase in the viscosity of the binder (approximately 16%) is observed when the C750 GnP content reaches or exceeds 0.05 wt%. As the testing temperature goes above 135 °C, the influence of C750 GnPs on the rotational viscosity of the binder becomes significantly less noticeable, and the differences in the viscosity values between the unmodified and modified binders become very marginal. For example, the addition of 1 wt% C750 GnPs to the binder results in only a 2.5% increase in the rotational viscosity. Hence, the effects of M15 and C750 GnPs on the viscosity of the binders are clearly divergent. One possible explanation for this observation is that GnPs with large mean particle diameters interact better with the asphalt components, hindering the movement of the particles, and resulting in more resistance to flow. It is worthwhile to measure the level of GnP dispersion in asphalt binder, though this measurement is extremely challenging and there are very few reports in the literature in this respect. For example, Wang et al. [34] used optical microscopy and 2D image processing to determine the GnP dispersion in asphalt binder. However, the reliability of this analysis becomes uncertain at lower GnP concentrations, and, therefore, no measurements were made of the level of GnP dispersion in the asphalt binders in this work. Nevertheless, the GnPs are believed to be well-dispersed in the asphalt binder samples herein since the results do not show appreciable variations with repeated measurements. It's important to note that an optimal GnP content typically exists for each GnP grade, beyond which the properties of the asphalt binder may deteriorate. Besides the GnP dispersion, the graphene-modified asphalt binder is recognized for its favorable colloidal stability, ensuring effective storage stability over time [35].

A comparison between the effect of the different GnP grades (C750, M15, M25, and R25) on the rotational viscosity of the asphalt binder at the constant GnP content of 1.0 wt% and different temperatures is provided in Fig. 3. As mentioned before, the M15 and M25 GnPs have similar thicknesses but different

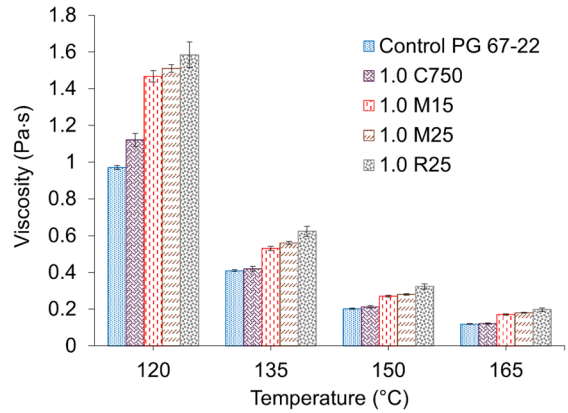


**Fig. 3** Effects of the different grades of GnPs on the rotational viscosity of the PG 67-22 asphalt binder at different temperatures. The GnP content is fixed at 1.0 wt% for all samples

lateral dimensions. Conversely, M25 and R25 GnPs have the same average lateral dimensions but differ in thicknesses and surface areas. The asphalt binder modified with R25 GnPs is observed to yield the highest rotational viscosity (Fig. 3), confirming that the larger the GnP mean particle diameter and thickness, the higher the GnP-modified binder viscosity. This observation provides evidence that the viscosity increase in the GnP-modified asphalt binder is attributed to the geometric characteristics of the GnPs. It is important to mention that, in accordance with the AASHTO standards, the rotational viscosity of the asphalt binder at 135 °C should be below 3 Pa s to ensure adequate workability of the asphalt mixture during pavement placement and compaction on the road. This criterion can still be met for all the GnP grades and contents used herein, suggesting that there are no detrimental effects on the asphalt mixture workability by incorporating GnPs in asphalt binders.

### 3.2 Rheological performance

The rutting parameters of the unaged GnP-modified asphalt binders are provided in Fig. 4. For the M15 GnPs, at all testing temperatures, as the content increases, the rutting parameter increases too with an optimal GnP content ranging from 1 to 1.5 wt%. At an M15 GnP content of 1.5 wt%, the rutting parameter increases by 53, 44.4, and 44.5% at temperatures of 64 °C, 70 °C, and 76 °C respectively (Fig. 4a). This observation can be attributed to the increase in the complex shear modulus (G*) and decrease in the phase angle (δ), brought about by the presence of M15 GnPs in the asphalt binder, as shown in the black diagram (Fig. 5). Overall, the inclusion of M15 GnPs in the asphalt binder results in higher complex shear modulus and a shift toward a lower phase angle, indicating an increase in its elastic response. As a consequence, the resistance of the binder to permanent deformation is enhanced [36]. Additionally, the improvement is less pronounced when the M15 GnP content exceeds 1.5 wt%, which could be attributed to a reduction in the GnP dispersion level. On the other hand, a slight improvement is observed in the rutting parameter when the binder is modified with C750 GnPs

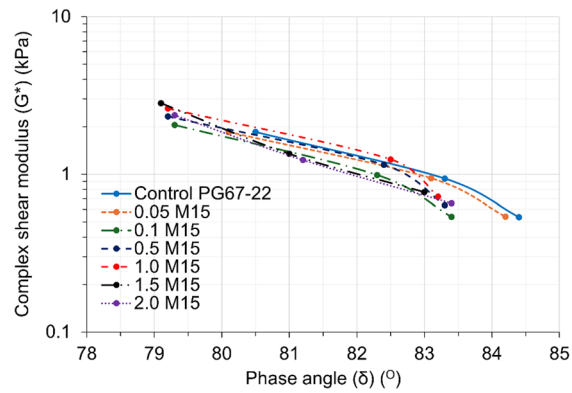


**Fig. 5** Rheological black diagrams for M15 GnP-modified asphalt binders

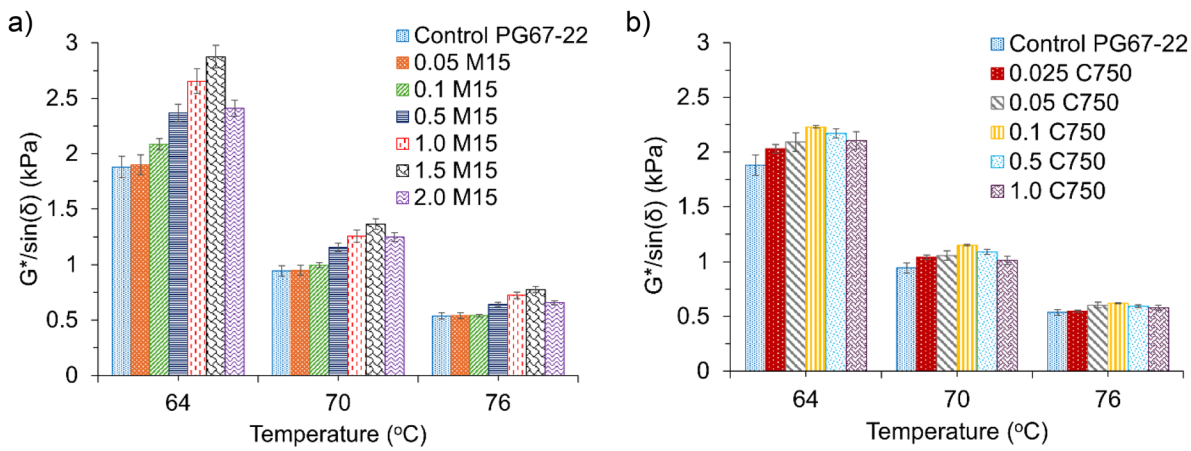


**Fig. 4** Effects of the different contents of **a** M15 GnPs and **b** C750 GnPs on the rutting parameter, i.e., G*/sin(δ), of the unaged PG 67-22 asphalt binder at different temperatures

(Fig. 4b). The optimal content for this GnP grade is 0.1 wt%, which corresponds to a rutting parameter increase of less than 18.6% at all temperatures. Thus, the overall performance of the asphalt binder modified with M15 GnPs is better than that modified with C750 GnPs. These results further highlight the significant role of the geometric characteristics of GnPs in enhancing the high-temperature performance of asphalt binders. It is postulated that large-diameter GnPs enable the creation of a more compact 3D network between the GnPs and asphalt components, resulting in decreased molecular mobility of the binder and, hence, improved rutting parameters [10, 33].

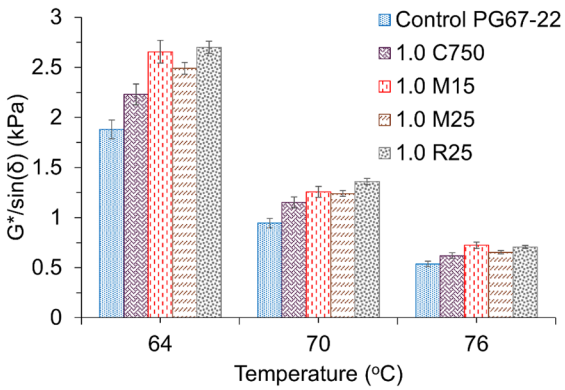


**Fig. 6** Rutting parameters of the unaged PG 67-22 asphalt binders modified with different GnP grades

In Fig. 6, the effect of the GnP grade/size on the rutting parameter of the GnP-modified asphalt binder is depicted. For this subgroup, the GnP content is fixed at 1 wt% for all GnP grades. In general, the rutting parameter is observed to be the highest for the asphalt binder containing R25 GnPs followed by M15, M25, and C750 GnPs. Once again, it is confirmed that the GnPs with large mean particle diameters are more effective in improving the rutting parameter of the asphalt binder. Additionally, it is observed that the surface areas of the GnPs do not influence the high-temperature properties of the GnP-modified asphalt binder.

The rutting parameters of the short-term aged GnP-modified binders are shown in Fig. 7. By considering the results of both the unaged and Rolling Thin-Film Oven (RTFO)-aged binders, it can be observed that the inclusion of only a small amount of the GnPs improves the high-temperature grade. For further analysis, the G* ratio (G* RTFO/G* unaged) was employed to evaluate the aging resistance of the binders [29, 30]. A lower G* ratio indicates a better anti-aging performance of the binder. In Fig. 8, the G* ratios of the GnP-modified samples at all testing temperatures are presented. In general, adding GnPs to the asphalt binder was observed to enhance its aging resistance across all temperatures, while the maximum anti-aging performance was achieved with the addition of M15 GnPs, as opposed to the C750 GnPs. These results demonstrate that the inclusion of 1.5 wt% M15 GnPs significantly improve the aging

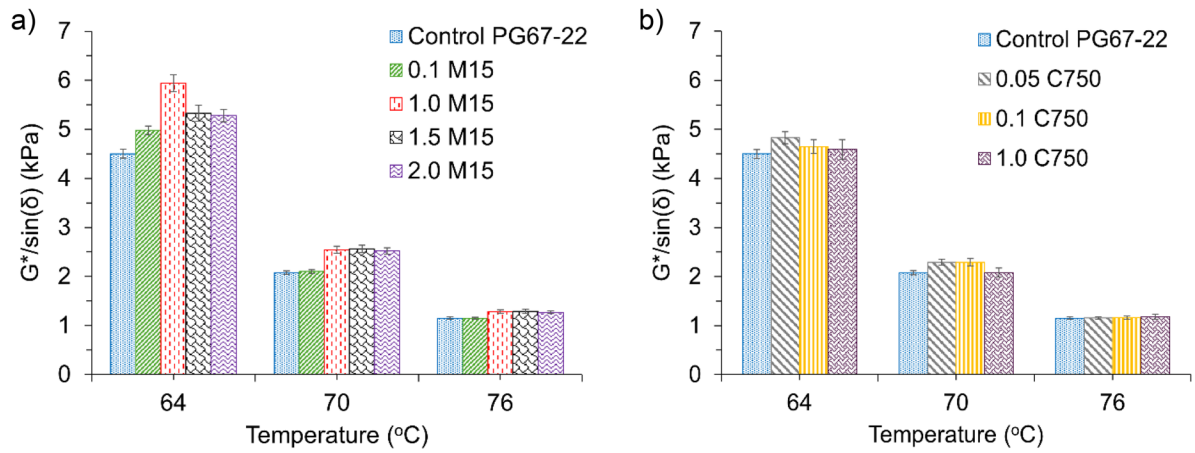


**Fig. 7** Effects of the different contents of **a** M15 GnPs and **b** C750 GnPs on the rutting parameter, i.e., G*/sin(δ), of the short-term aged PG 67-22 asphalt binder at different temperatures

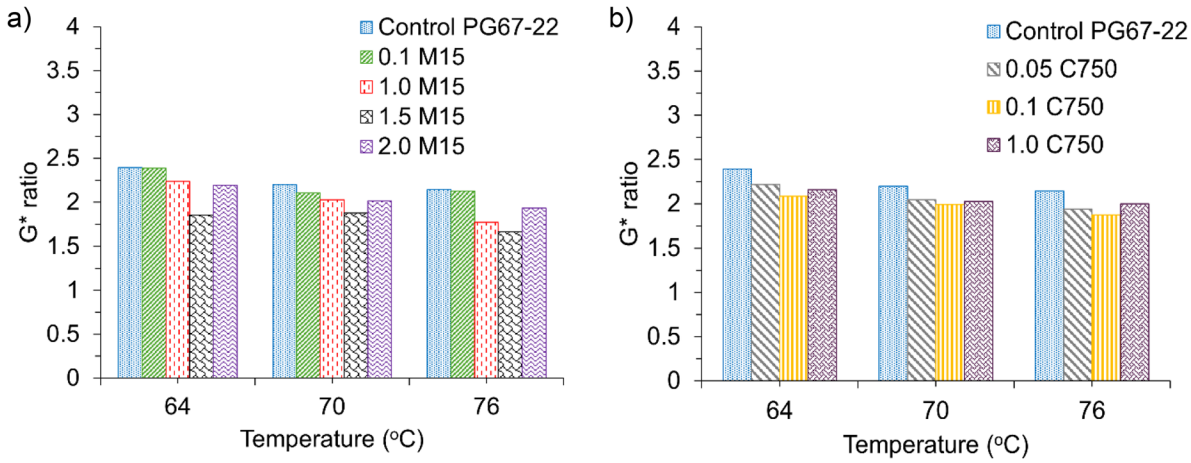


**Fig. 8** Effects of the different contents of **a** M15 GnPs and **b** C750 GnPs on the G* ratios of the short-term aged PG 67-22 asphalt binder at different temperatures

resistance of the asphalt binder. Based on literature, GnPs may act as micellar nuclei in asphalt and graphene sheets can impede and/or prevent the diffusion of oxygen into asphalt binder [8]. Moreover, there is computational evidence that graphene sheets inhibit the oxidation of saturated phenols and, thereby, improve the aging resistance of asphalt [37].

To highlight the significant effect of GnPs on the rutting performance of asphalt binder, a comparison was made between the properties of a GnP-modified asphalt binder and a control polymer-modified binder. For this purpose, the PG 67-22 asphalt binder was modified with 2.0 wt% high-density polyethylene (HDPE), and its rutting performance was compared to those of GnP-modified binders with 1.0, 1.5, and 2.0 wt% M15 GnPs. The results are presented in Fig. 9. Notably, the performance of the M15 GnP-modified asphalt binder was observed to surpass that of HDPE at GnP contents of 1.0–1.5 wt% at nearly all temperatures (Fig. 9).

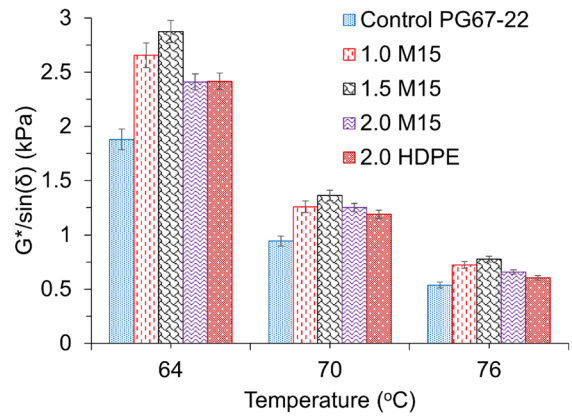


**Fig. 9** Effects of the different contents of M15 GnPs and a control HDPE modifier (2.0 wt%) on the G* ratios of the PG 67-22 asphalt binder at different temperatures

### 3.3 MCSR results

The MSCR test was also performed to assess the rutting performance of the asphalt samples. The results are presented in terms of the unrecoverable creep compliance ($J_{nr}$) and the percent recovery $R_{\%}$. $J_{nr}$ can be utilized as an indicator of permanent deformation, while $R_{\%}$ represents the elastic response. In Fig. 10, the MSCR findings for the M15 GnP-modified binders at two temperatures of 64 and 70 °C are shown. The results indicate that adding M15 GnPs to the asphalt binder significantly reduces its permanent deformation. At both temperatures, the presence of GnPs notably reduces the $J_{nr}$ and increases the $R_{\%}$ of the binder, signifying improvements in its rutting resistance and elastic behavior. For example, at 70 °C, adding 1.5 wt% M15 GnPs to the binder can reduce the $J_{nr}$ by 33.2% and increase the $R_{\%}$ by 53.9%. Herein, the optimal content of M15 GnPs was found to be between 1 to 1.5 wt%. The reduction of $J_{nr}$ can be attributed to

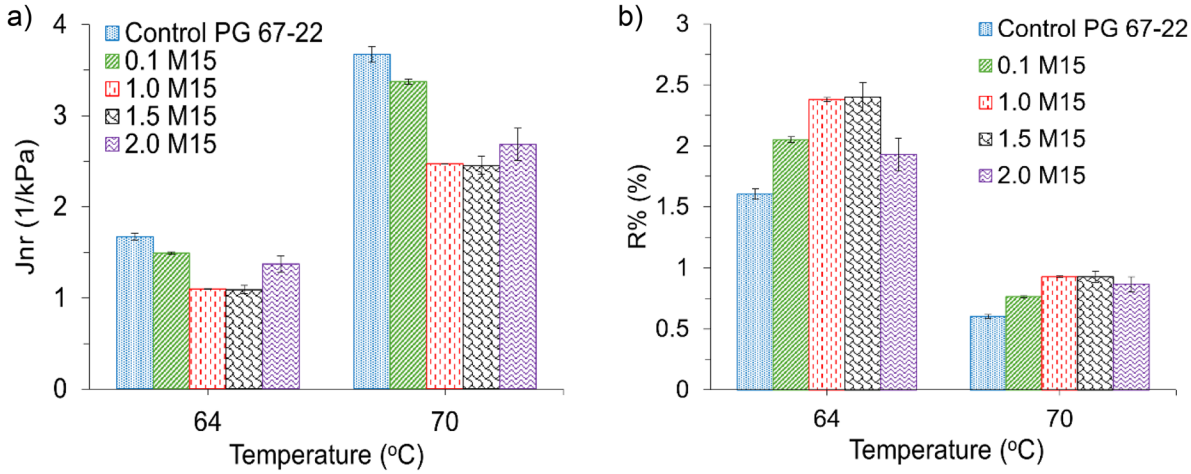


**Fig. 10** MSCR test results, **a** $J_{nr}$ and **b** $R_{\%}$, of the M15 GnP-modified asphalt binders at a stress of 3.2 kPa and different GnP contents and temperatures

the ability of the GnPs to improve the binder stiffness, leading to a significant reduction of the permanent deformation in the binder. Additionally, GnPs enhance the aging resistance and anti-aging properties of the binder, which can lead *J*to a more elastic short-term aged binder. On the contrary, the impact of C750 GnPs (Fig. 11) on $_{nr}$ and $R_{\%}$ is observed to be negligible. Furthermore, changing the content of C750 GnPs does not result in any substantial improvement in the $J_{nr}$ or $R_{\%}$ values of the binder.

The observed improvements in the MSCR results of the GnP-modified asphalt binder can be evaluated with reference to the AASHTO M332 binder specification requirements. In this context, the control binder is graded as PG 64S, a standard grade in a 64 °C maximum pavement design temperature climate. Therefore, the asphalt binders with 0.1, 1.0, 1.5, and 2.0 wt% M15 GnP contents would all be graded as PG 70S, the standard grade in a 70 °C climate. Since the control asphalt binder is quite close to meeting the 70S requirements, this is a small

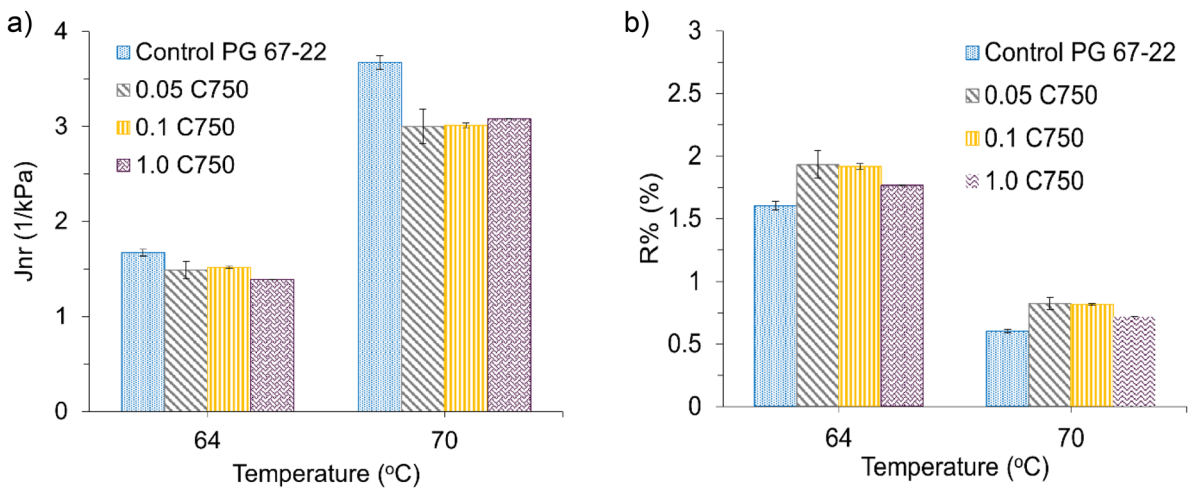


**Fig. 11** MSCR test results, **a** $J_{nr}$ and **b** $R_{\%}$, of the C750 GnP-modified asphalt binders at a stress of 3.2 kPa and different GnP contents and temperatures

difference from a pavement design perspective. However, the binders with 0.05, 0.1, and 1.0 wt% C750 GnPs exhibit sufficient improvement in the $J_{nr}$ values to meet the requirements for a 70H or heavy traffic grade in a 70 °C climate.

### 3.4 FTIR results

The chemical structures of the neat and GnP-modified asphalt binders were analyzed using ATR-FTIR spectroscopy. In addition, the potential interactions at the binder-GnP interface were also monitored using this technique. Typical ATR-FTIR spectra of the unaged samples are shown in Fig. 12. The samples were observed to exhibit similar peaks in terms of shape, intensity, and position, supporting the formation of a homogenous asphalt binder structure. Specifically, the C-H bond stretching and bending vibrations were observed in the region of 2924–2851 and 1452–1373 $cm^{-1}$ respectively, which confirms the presence of saturated hydrocarbons in the asphalt compounds. The C=C stretching vibration appeared at 1602 $cm^{-1}$, which reveals the presence of the corrugated vibration of the benzene ring, corresponding to the aromatic compounds in the asphalt binders. The absorption bands of GnPs were completely absent from the FTIR spectra due to the overwhelming effect of the asphalt binder spectrum over that of the GnP due to the very low GnP contents incorporated in the binders. Furthermore, no variations in the peak positions or intensities were detected upon GnP incorporation in the binder, similar to the findings of Li et al. [10]. Therefore, it can be concluded that GnPs did not alter the structural integrity of the asphalt binder. They were merely dispersed in the asphalt matrix and established noncovalent π-π interactions between the aromatic components of the asphalt binder and the $sp^2$-hybridized GnPs.

### 3.5 AFM results

Because the optimum GnP content was found to be between 1.0 and 1.5 wt% M15 GnPs, these M15 GnP-modified binder samples were selected for AFM imaging and compared to the control, as well as the 0.1 and 1.0 wt% C750 GnP-modified binders. In Fig. 13, the height image of the control sample is shown, where three relative phase distinct regions can be distinguished: the Catana, Peri, and Para phases. Each phase exhibits different characteristics, such as elastic modulus, adhesion, and refractive index [38, 39]. The Catana phase, known as the "bee" structure, corresponds to the wave-like microstructure on the binder surface. The Peri phase, or the resin, is the phase surrounding the bee structure (slightly recessed) and is relatively stiff. The Para phase is characterized as the flat and softest phase present on the asphalt surface [38, 39]. In general, the Peri phase is relatively stiffer than the Para phase, while the Catana phase may show both hard and soft domains [39].

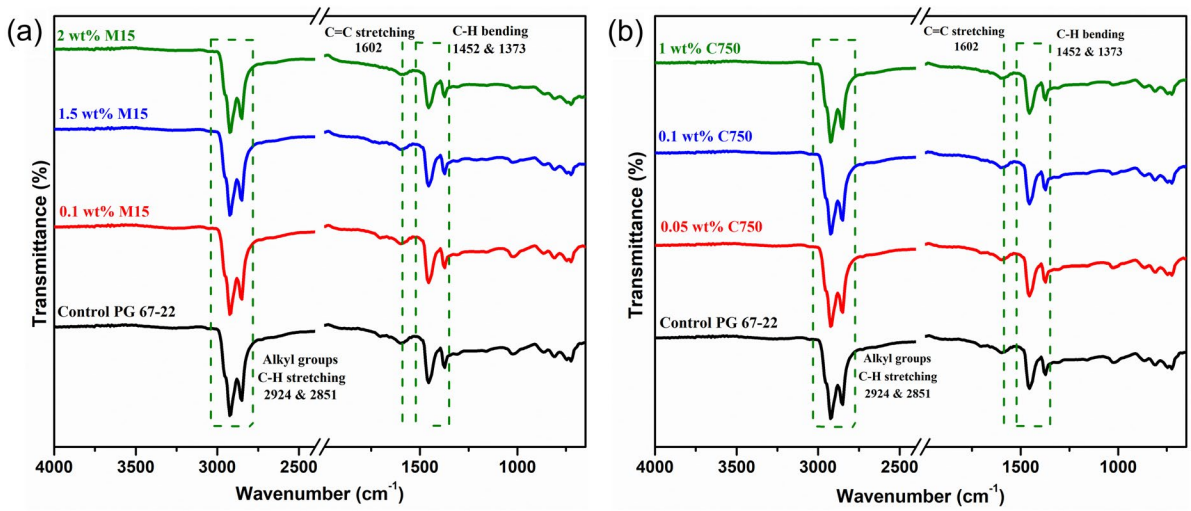


**Fig. 12** FTIR spectra of the unaged **a** M15 GnP-modified binders and **b** C750 GnP-modified binders

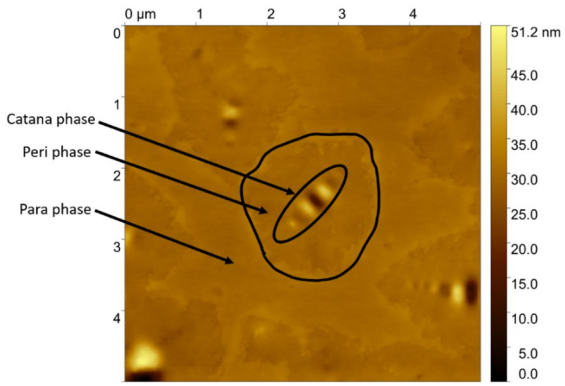


**Fig. 13** AFM image of the neat PG 67-22 asphalt binder (control sample-no graphene)

It has been shown that adjusting the tapping force of the probe can produce high-contrast phase images of the Peri and Para phases of asphalt binder [40]. To quantify the effect of the addition of GnPs to asphalt binder on its morphological properties, Otsu's method of image thresholding [41] was adopted to create a mask of the Peri phase from which the projected surface area (PSA) of the mask was calculated. The PSA indicates changes in the size and number of the Peri phase surrounding the bee structures. In Fig. 14, the phase and masked images of the neat and GnP-modified binder samples are shown. Moreover, in Fig. 15 the calculated PSA of the Peri and Catana phases are presented. One significant observation is that the Peri phase is softer than the Para phase in the C750 GnP-modified binders. This is indirect contrast to the reports in the literature for unmodified binders, as well as findings presented here for the control and M15 GnP-modified binders. This needs to be explored further. Additionally, the C750 GnPs reduced the PSA of the Peri/Catana phases in comparison to the control, with a 13.7% and 3.4% reduction observed for the binders modified with 0.1 and 1.0 wt%, respectively. There is no significant difference in the rotational viscosity for these two samples. Interestingly, the C750 GnP-modified binder with 0.1 wt% GnPs, which had the greatest reduction in the PSA, is the optimal C750 GnP-modified binder sample for the rutting parameter. The 1.0 wt% M15 GnP-modified binder had the largest PSA, with an 11% increase from the control, though there was also a moderate increase of 5.2% in the PSA of the 1.5 wt% M15 GnP-modified binder. In contrast to the C750 GnP-modified binder, this shows a positive correlation between the increase in the PSA of the M15 GnP-modified binder and the increase in its rotational viscosity, as well as the rutting parameter. More work needs to be done to explore and explain these relationships.

## 4 Conclusion

In this work, the effect of the geometric characteristics of GnPs on the high-temperature performance of asphalt binder PG 67-22 was investigated. Four GnP grades with different mean particle diameters, i.e., xGnP® M15, M25, R25, and C750, were utilized to modify the asphalt binder. The GnP content varied between 0.05 and 2 wt%. The results demonstrated that GnPs with large mean particle diameters, such as M15, have a more pronounced effect on the high-temperature performance of the asphalt binder than the small-size ones, such as C750. The former causes an increase in the binder viscosity and enhancement in several other binder characteristics, including the rutting parameter, resistance to permanent deformation, and elastic recovery. Moreover, they enhance the short-term anti-aging properties of the asphalt binder, possibly by acting as a gas barrier, impeding the diffusion of the oxygen molecules into the binder. The GnPs with smaller mean particle diameters have a negligibly small effect on the high-temperature performance of the binder. The FTIR results indicate that only noncovalent π-π interactions exist between the aromatic components of the asphalt binder and the GnPs. The absence of absorption bands of GnPs in the FTIR spectra is attributed to the overwhelming influence of asphalt binder, resulting from the very low GnP contents. Based on the obtained AFM images, the GnPs with large mean particle diameters can increase the projected surface area of the Peri/Catana phases, while those with small mean particle diameters have the opposite effect.

(a) Control PG 67-22

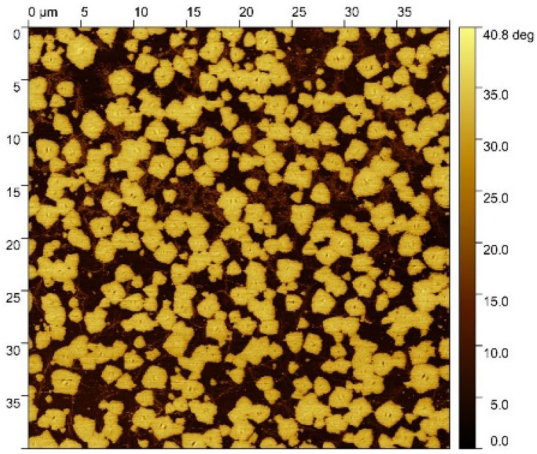


(b) 0.1 C750

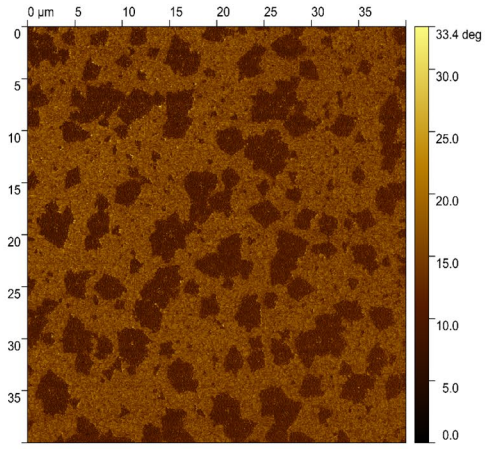


(c) 1.0 C750

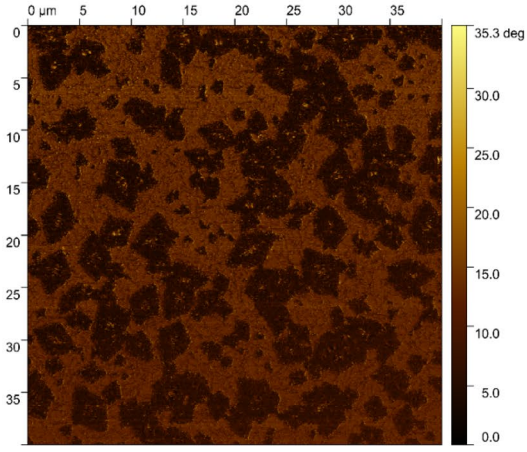


(d) 1.0 M15

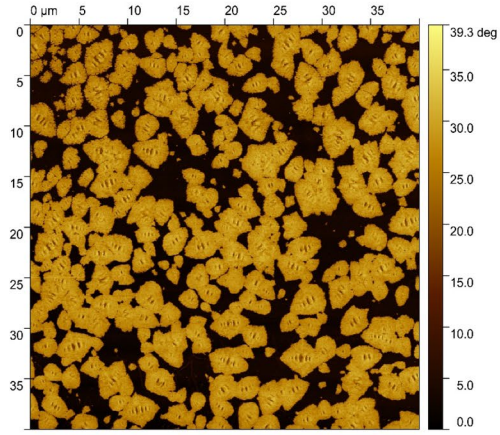


(e) 1.5 M15

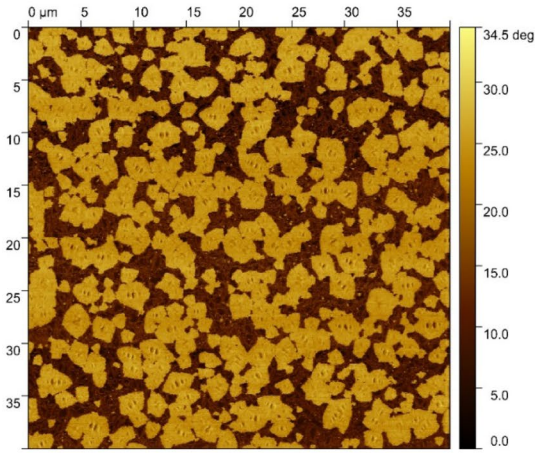

◂**Fig. 14** AFM phase and masked contrast phase images of unaged **a** control PG 67-22 asphalt binder, **b** 0.1 C750, **c** 1.0 C750, **d** 1.0 M15, and **e** 1.5 M15 GnP-modified binder

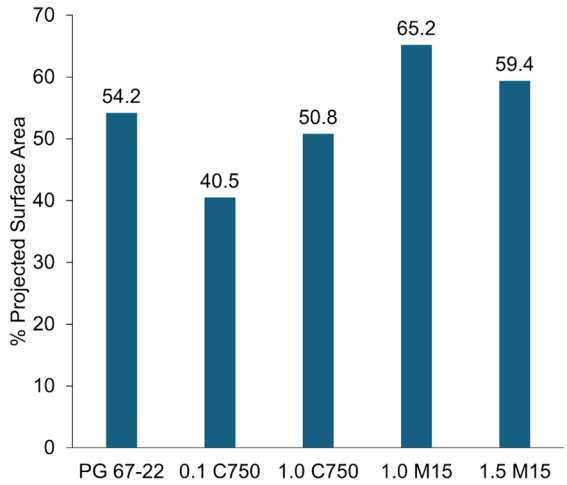


**Fig. 15** Percent projected surface area of Peri/Catana phases of the neat and GnP-modified asphalt binders, as determined by AFM contrast phase images

**Acknowledgements** The work described in this document was conducted in the Center for Graphene Research and Innovation at the University of Mississippi. The authors acknowledge the support provided by the U.S. Army Engineer Research and Development Center (ERDC) and the Military Engineering Research and Development Area under contract W912HZ21C0040. Permission to publish was granted by the ERDC Geotechnical and Structures Laboratory.

**Funding** The research described and the resulting data presented herein, unless otherwise noted, were funded under CA BO340 497014 Project, "Graphene Applications for Military Engineering," under Contract W912HZ21C0040, and managed by the U.S. Army Engineer Research and Development Center (ERDC).

**Declarations**

**Conflict of interest** The authors declare that they have no known competing financial interests or personal relationships that could have appeared to influence the work reported in this paper.



## References

1. Li M, Xu O, Min Z, Wang Q (2023) Engineering performance and activation mechanism of asphalt binder modified by microwave and diesel pre-processed waste crumb rubber. Mater Struct/Mater Constr. https://doi.org/10.1617/s11527-023-02204-x
2. Venudharan V, Biligiri KP (2017) Effect of crumb rubber gradation on asphalt binder modification: rheological evaluation, optimization and selection. Mater Struct/Mater Constr. https://doi.org/10.1617/s11527-017-0994-x
3. Zheng W, Wang H, Chen Y et al (2021) A review on compatibility between crumb rubber and asphalt binder. Constr Build Mater 297. https://doi.org/10.1016/j.conbuildmat.2021.123820
4. Behnood A, Modiri Gharehveran M (2019) Morphology, rheology, and physical properties of polymer-modified asphalt binders. Eur Polym J 112:766–791
5. Wang T, Xu G, Gong M et al (2021) Full range temperature susceptibility of aged bitumen rejuvenated by polymer modified bio-derived rejuvenator. Mater Struct/Mater Constr. https://doi.org/10.1617/s11527-021-01692-z
6. Isacsson U, Zeng H (1998) Low-temperature cracking of polymer-modified asphalt. Mat Struct 31:58–63. https://doi.org/10.1007/BF02486415
7. Li Y, Hao P, Zhao C et al (2021) Anti-rutting performance evaluation of modified asphalt binders: a review. J Traff Transp Eng (Engl Ed) 8:339–355
8. Li X, Wang YM, Wu YL et al (2021) Properties and modification mechanism of asphalt with graphene as modifier. Constr Build Mater. https://doi.org/10.1016/j.conbuildmat.2020.121919
9. Segundo IR, Landi S, Margaritis A et al (2020) Physicochemical and rheological properties of a transparent asphalt binder modified with nano-TiO2. Nanomaterials 10:2152. https://doi.org/10.3390/NANO10112152
10. Li X, Wang YM, Wu YL et al (2021) Properties and modification mechanism of asphalt with graphene as modifier. Constr Build Mater 272:121919. https://doi.org/10.1016/J.CONBUILDMAT.2020.121919
11. Tanzadeh J, Vahedi F, Pezhouhan TK, Tanzadeh R (2013) Laboratory study on the effect of nano TiO2 on rutting performance of asphalt pavements. Adv Mat Res 622–623:990–994. https://doi.org/10.4028/WWW.SCIENTIFIC.NET/AMR.622-623.990
12. Shafabakhsh GH, Ani OJ (2015) Experimental investigation of effect of Nano TiO2/SiO2 modified bitumen on the rutting and fatigue performance of asphalt mixtures containing steel slag aggregates. Constr Build

Mater 98:692–702. https://doi.org/10.1016/J.CONBUILDMAT.2015.08.083
13. You Z, Mills-Beale J, Foley JM et al (2011) Nanoclay-modified asphalt materials: preparation and characterization. Constr Build Mater 25:1072–1078. https://doi.org/10.1016/J.CONBUILDMAT.2010.06.070
14. Bagshaw SA, Kemmitt T, Waterland M, Brooke S (2018) Effect of blending conditions on nano-clay bitumen nanocomposite properties. Road Mater Pavem Des 20:1735–1756. https://doi.org/10.1080/14680629.2018.1468802
15. Enieb M, Diab A (2017) Characteristics of asphalt binder and mixture containing nanosilica. Int J Pavem Res Technol 10:148–157. https://doi.org/10.1016/J.IJPRT.2016.11.009
16. Hamedi GH, Nejad FM, Oveisi K (2016) Estimating the moisture damage of asphalt mixture modified with nano zinc oxide. Mater Struct/Mater Constr 49:1165–1174. https://doi.org/10.1617/s11527-015-0566-x
17. Khattak MJ, Khattab A, Rizvi HR (2011) Mechanistic characteristics of asphalt binder and asphalt matrix modified with nano-fibers. https://doi.org/10.1061/41165(397)492
18. Rizvi HR, Khattak MJ, Madani M, Khattab A (2016) Piezoresistive response of conductive Hot Mix Asphalt mixtures modified with carbon nanofibers. Constr Build Mater 106:618–631. https://doi.org/10.1016/J.CONBUILDMAT.2015.12.187
19. Faramarzi M, Arabani M, Haghi AK, Mottaghitalab V (2015) Carbon nanotubes-modified asphalt binder: preparation and characterization. Int J Pavem Res Technol 8:29–37. https://doi.org/10.6135/ijprt.org.tw/2015.8(1).29
20. Goli A, Ziari H, Amini A (2017) Influence of carbon nanotubes on performance properties and storage stability of SBS modified asphalt binders. J Mater Civ Eng 29:04017070. https://doi.org/10.1061/(ASCE)MT.1943-5533.0001910
21. Ahmad Nazki M, Chopra T, Chandrappa AK (2020) Rheological properties and thermal conductivity of bitumen binders modified with graphene. Constr Build Mater 238:117693. https://doi.org/10.1016/J.CONBUILDMAT.2019.117693
22. He J, Hu W, Xiao R et al (2022) A review on Graphene/GNPs/GO modified asphalt. Constr Build Mater 330:127222. https://doi.org/10.1016/J.CONBUILDMAT.2022.127222
23. Brcic H (2016) Investigation of the rheological properties of asphalt binder containing graphene nanoplatelets 41
24. Moreno-Navarro F, Sol-Sánchez M, Gámiz F, Rubio-Gámez MC (2018) Mechanical and thermal properties of graphene modified asphalt binders. Constr Build Mater 180:265–274. https://doi.org/10.1016/J.CONBUILDMAT.2018.05.259
25. Singh D, Kuity A, Girimath S et al (2020) Investigation of chemical, microstructural, and rheological perspective of asphalt binder modified with graphene oxide. J Mater Civ Eng 32:04020323. https://doi.org/10.1061/(ASCE)MT.1943-5533.0003385
26. Adnan AM, Lü C, Luo X, Wang J (2021) High-temperature rheological characteristics of asphalt binder incorporated with graphene oxide and predicting its rutting potential using response surface method. J Mater Civ Eng 33:04021331. https://doi.org/10.1061/(ASCE)MT.1943-5533.0003957
27. Zeng Q, Liu Y, Liu Q et al (2020) Preparation and modification mechanism analysis of graphene oxide modified asphalts. Constr Build Mater 238:117706. https://doi.org/10.1016/J.CONBUILDMAT.2019.117706
28. Huang G, He J, Zhang X et al (2021) Applications of Lambert-Beer law in the preparation and performance evaluation of graphene modified asphalt. Constr Build Mater 273:121582. https://doi.org/10.1016/J.CONBUILDMAT.2020.121582
29. Wang R, Yue J, Li R, Sun Y (2019) Evaluation of aging resistance of asphalt binder modified with graphene oxide and carbon nanotubes. J Mater Civ Eng 31:04019274. https://doi.org/10.1061/(ASCE)MT.1943-5533.0002934
30. Hafeez M, Ahmad N, Kamal MA et al (2019) Experimental investigation into the structural and functional performance of graphene nano-platelet (GNP)-doped asphalt. Appl Sci 9:686. https://doi.org/10.3390/APP9040686
31. Zhang X, He JX, Huang G et al (2019) Preparation and characteristics of ethylene bis(stearamide)-based graphene-modified asphalt. Materials 12:757. https://doi.org/10.3390/MA12050757
32. Shishehbor M, Pouranian MR, Ramezani MG (2019) Molecular investigations on the interactions of graphene, crude oil fractions and mineral aggregates at low, medium and high temperatures. Pet Sci Technol 37:804–811. https://doi.org/10.1080/10916466.2019.1566254
33. Liu K, Zhang K, Shi X (2018) Performance evaluation and modification mechanism analysis of asphalt binders modified by graphene oxide. Constr Build Mater 163:880–889. https://doi.org/10.1016/J.CONBUILDMAT.2017.12.171
34. Wang Y, Polaczyk P, He J et al (2022) Dispersion, compatibility, and rheological properties of graphene-modified asphalt binders. Constr Build Mater. https://doi.org/10.1016/j.conbuildmat.2022.128886
35. Huang Y, Wu Z, Liang L et al (2023) Revealing the dependance of mechanical properties of asphalt binder on graphene size via multi-scale methods. Mater Des. https://doi.org/10.1016/j.matdes.2023.112478
36. Liu S, Mo L, Wang K et al (2016) Preparation, microstructure and rheological properties of asphalt sealants for bridge expansion joints. Constr Build Mater 105:1–13. https://doi.org/10.1016/j.conbuildmat.2015.12.017
37. Liao M, Gao Y, Xie Y et al (2022) Investigation on the anti-aging properties enhancement mechanism of graphene on RA based on size effect. Case Stud Constr Mater. https://doi.org/10.1016/j.cscm.2022.e01634
38. Saha R, Malloy K, Bautista E, Sobolev K (2017) The investigation of fly ash based asphalt binders using atomic force microscope. Front Struct Civ Eng 11:380–387. https://doi.org/10.1007/S11709-017-0437-3/METRICS
39. Zhang M, Hao P, Dong S et al (2020) Asphalt binder micro-characterization and testing approaches: a review. Measurement 151:107255. https://doi.org/10.1016/J.MEASUREMENT.2019.107255
40. Hung AM, Fini EH (2015) AFM study of asphalt binder "bee" structures: origin, mechanical fracture, topological evolution, and experimental artifacts. RSC Adv 5:96972–96982. https://doi.org/10.1039/C5RA13982A

41. Liu D, Yu J (2009) Otsu method and K-means. In: Proceedings—2009 9th international conference on hybrid intelligent systems, HIS 2009, vol 1, pp 344–349. https://doi.org/10.1109/HIS.2009.74